

Discriminating 1D new physics solutions in $b \rightarrow s\ell\ell$ decays

Shuang-Yi Li,¹ Rui-Xiang Shi,¹ and Li-Sheng Geng^{2,3,*}

¹*School of Physics, Beihang University, Beijing 102206, China*

²*School of Physics & Beijing Key Laboratory of Advanced Nuclear Materials and Physics,
Beihang University, Beijing 102206, China*

³*School of Physics and Microelectronics,
Zhengzhou University, Zhengzhou, Henan 450001, China*

Abstract

The recent measurements of R_{K^+} , $R_{K_S^0}$, $R_{K^{*+}}$, $B_s \rightarrow \mu^+\mu^-$, a set of CP-averaged angular observables for the $B^0 \rightarrow K^{*0}\mu^+\mu^-$ decay, and its isospin partner $B^+ \rightarrow K^{*+}\mu^+\mu^-$ by the LHCb Collaboration, consistently hint at lepton universality violation in the $b \rightarrow s\ell\ell$ transitions. In this work, we first perform global fits to the $b \rightarrow s\ell\ell$ data and show that five one-dimensional scenarios, i.e. δC_9^μ , δC_{10}^μ , δC_L^μ , $\delta C_9^\mu = C_{10}^{\mu'}$, and $\delta C_9^\mu = -C_9^{\mu'}$ can best explain the so-called B anomalies. Furthermore, we explore how these scenarios can be distinguished from each other. For this purpose, we first study the combinations of four angular asymmetries A_i ($i = 3, 4, 5, 9$) and find that they cannot distinguish the five new physics scenarios. We then show that a newly constructed ratio R_S can uniquely discriminate the five new physics scenarios in proper intervals of q^2 if it can be measured with a percent level precision.

* E-mail:lisheng.geng@buaa.edu.cn

I. INTRODUCTION

In the standard model (SM), the rare decays of B mesons induced by flavour-changing neutral-current (FCNC) $b \rightarrow s\ell\ell$ transition at the quark level are suppressed by the GIM mechanism [1]. Therefore they provide an ideal laboratory to indirectly probe new physics (NP) beyond the SM. Interestingly, the measurements of several observables yield results in tension with the SM expectations (see Refs. [2, 3] for recent reviews).

Recently, the LHCb Collaboration reported the most precise measurement of $R_{K^+} = \Gamma(B^+ \rightarrow K^+\mu^+\mu^-)/\Gamma(B^+ \rightarrow K^+e^+e^-)$ in the bin [1.1, 6] GeV² [4]

$$R_{K^+} = 0.846_{-0.039-0.012}^{+0.042+0.013}, \quad (1)$$

showing that the significance of deviation from the SM prediction (see Table 1 in Ref. [5]) is at 3.1σ confidence level. Compared to the 2014 measurement [6], the tension with respect to the SM prediction has significantly increased. At the same time, a new result for the $B_s \rightarrow \mu^+\mu^-$ branching fraction,

$$\text{BR}(B_s^0 \rightarrow \mu^+\mu^-) = (3.09_{-0.43-0.11}^{+0.46+0.15}) \times 10^{-9}, \quad (2)$$

is also published by the LHCb Collaboration [7, 8], which allows for a better constraint on the Wilson coefficient C_{10} . In Ref. [9], together with the theoretical prediction of Ref. [10] including the double-logarithmic QED and QCD corrections, the CMS measurement [11], and the ATLAS measurement [12], the following ratio is obtained

$$R = \frac{\text{BR}(B_s^0 \rightarrow \mu^+\mu^-)_{\text{exp}}}{\text{BR}(B_s^0 \rightarrow \mu^+\mu^-)_{\text{SM}}} = 0.78(9). \quad (3)$$

Very recently, the LHCb Collaboration measured two new lepton-universality ratios $R_{K_S^0} = \Gamma(B^0 \rightarrow K_S^0\mu^+\mu^-)/\Gamma(B^0 \rightarrow K_S^0e^+e^-)$ and $R_{K^{*+}} = \Gamma(B^+ \rightarrow K^{*+}\mu^+\mu^-)/\Gamma(B^+ \rightarrow K^{*+}e^+e^-)$ in the q^2 ranges [1.1, 6.0] GeV² and [0.045, 6.0] GeV², respectively, using proton-proton collision data corresponding to an integrated luminosity of 9 fb⁻¹ [13]. The two ratios are

$$\begin{aligned} R_{K_S^0} &= 0.66_{-0.14-0.04}^{+0.20+0.02}, \\ R_{K^{*+}} &= 0.70_{-0.13-0.04}^{+0.18+0.03}, \end{aligned} \quad (4)$$

where the first error is statistical and the second is systematic. We note that the central values are close to the Belle measurements [14, 15], but the uncertainties are smaller, resulting in deviations from the SM predictions with a significance of 1.5σ and 1.4σ , respectively.

On the other hand, in 2020 the LHCb Collaboration reported angular analyses of the $B^0 \rightarrow K^{*0}\mu^+\mu^-$ decay and its isospin partner $B^+ \rightarrow K^{*+}\mu^+\mu^-$ decay [16, 17]. The results reconfirm the global tension with respect to the SM predictions previously reported for the decay of $B^0 \rightarrow K^{*0}\mu^+\mu^-$ [18].

These new measurements have attracted much attention and led to many model-independent global analyses [9, 19–30] assuming the presence of NP only in the $b \rightarrow s\mu^+\mu^-$ mode, and it is shown that the significance of the SM exclusion in the global fits is about $4 \sim 6\sigma$. These data have also been explained in NP models involving tree-level exchanges of new particles such as the neutral gauge boson Z' [31–40], leptoquarks [20, 21, 25, 41–51] or scalar Higgs [52, 53]. It is interesting to note that the leptoquark models can simultaneously explain the $b \rightarrow s\ell^+\ell^-$ (with $\ell = e, \mu$) and charged current (CC) $b \rightarrow c\ell^-\bar{\nu}_\ell$ (with $\ell = \mu, \tau$) flavor anomalies [20, 21, 25, 43, 46, 49, 54].

The so-called B anomalies can be best explained in five one-dimensional scenarios, i.e. $\delta C_9^\mu, \delta C_{10}^\mu, \delta C_L^\mu, \delta C_9^\mu = C_{10}^{\mu'}$, and $\delta C_9^\mu = -C_9^{\mu'}$, as demonstrated in the model independent analyses [9, 19–23, 25, 26, 29, 55–66]. In this work, assuming that NP appears in the muon mode¹, we first present global fits to the $b \rightarrow s\ell^+\ell^-$ data for the SM and five one-dimensional NP scenarios $\delta C_9^\mu, \delta C_{10}^\mu, \delta C_L^\mu, \delta C_9^\mu = C_{10}^{\mu'}$, and $\delta C_9^\mu = -C_9^{\mu'}$, the latter two were not considered in Ref. [9]. Next, we study the four angular asymmetries A_i ($i = 3, 4, 5, 9$) and find that they cannot discriminate the five new physics scenarios. Finally, we show that a set of ratios R_i are helpful to uniquely discriminate the NP scenarios. In addition, we present predictions in the SM and different NP scenarios for binned observables A_i and R_i in certain ranges of bins, which might be relevant for future experiments.

This work is organized as follows. We introduce the observables A_i and R_i in Sec. II. Results and discussions are given in Sec. III, followed by a short summary and outlook in Sec. IV.

II. ANGULAR OBSERVABLES A_i AND R_i FOR THE $B \rightarrow K^*\ell^+\ell^-$ DECAY

For details about our theoretical framework, the low-energy effective Hamiltonian, the origin of theoretical uncertainties and how they are parameterized, and the statistical methods used to perform global fits to all the relevant experimental data, we refer to Ref. [9]. In this section, we introduce some angular observables which can potentially discriminate different NP scenarios. For this, we focus on the $B \rightarrow K^*\ell^+\ell^-$ decay. The differential decay rate for the four-body $B(p) \rightarrow K^*(k)(\rightarrow K\pi)\ell^+(q_1)\ell^-(q_2)$ decay is of the following form [67, 68]

$$\frac{d^{(4)}\Gamma}{dq^2 d \cos \theta_\ell d \cos \theta_K d\phi} = \frac{9}{32\pi} I^{(\ell)}(q^2, \theta_\ell, \theta_K, \phi), \quad (5)$$

¹ For a discussion about the scenario where NP appears in both the electron and muon channels, see Appendix A.

with

$$\begin{aligned}
I^{(\ell)}(q^2, \theta_\ell, \theta_K, \phi) = & (I_1^s \sin^2 \theta_K + I_1^c \cos^2 \theta_K + (I_2^s \sin^2 \theta_K + I_2^c \cos^2 \theta_K) \cos 2\theta_\ell \\
& + I_3 \sin^2 \theta_K \sin^2 \theta_\ell \cos 2\phi + I_4 \sin 2\theta_K \sin 2\theta_\ell \cos \phi \\
& + I_5 \sin 2\theta_K \sin \theta_\ell \cos \phi \\
& + (I_6^s \sin^2 \theta_K + I_6^c \cos^2 \theta_K) \cos \theta_\ell + I_7 \sin 2\theta_K \sin \theta_\ell \sin \phi \\
& + I_8 \sin 2\theta_K \sin 2\theta_\ell \sin \phi + I_9 \sin^2 \theta_K \sin^2 \theta_\ell \sin 2\phi), \tag{6}
\end{aligned}$$

where the kinematic variables q^2 , θ_ℓ , θ_K and ϕ are defined, respectively, as follows: (i) $q^2 = (p - k)^2$ is the square of the dilepton invariant mass, (ii) θ_ℓ is the angle between the flight direction of the B meson and the ℓ^- lepton in the dilepton rest frame, (iii) θ_K is the angle between momenta of the B meson and the K meson in the dimeson ($K\pi$) rest frame, (iv) ϕ is the angle between the dimeson ($K\pi$) and dilepton rest frames. As shown in Fig. 1, both θ_ℓ and θ_K are defined in the interval $[0, \pi]$ while the range of ϕ is $[0, 2\pi]$. The angular coefficients I_i expressed in terms of the helicity amplitudes can be found in Ref. [68], while the expressions of the CP-conjugate decay $\bar{B} \rightarrow \bar{K}^* \ell^+ \ell^-$ can be obtained by the following replacements

$$I_{1s(c),2s(c),3,4,7} \rightarrow \bar{I}_{1s(c),2s(c),3,4,7}, \quad I_{5,6,8,9} \rightarrow -\bar{I}_{5,6,8,9}, \tag{7}$$

where $\bar{I}_i = I_i^*$.

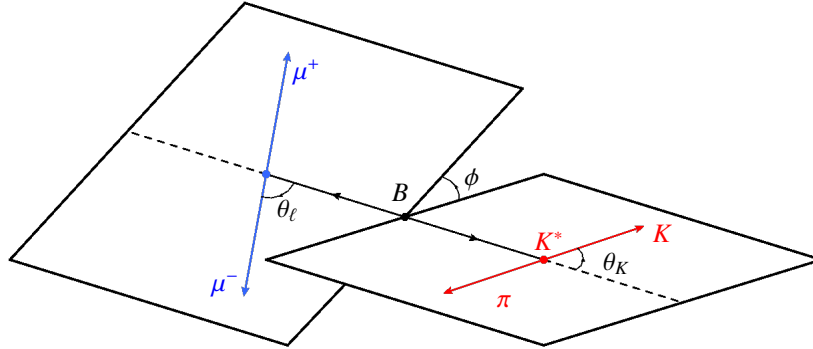


FIG. 1. Kinematics of the $B \rightarrow K^* \ell^+ \ell^-$ decay.

Following the strategy outlined in Refs. [69, 70], we can “construct” four angular asymmetries A_i ($i = 3, 4, 5, 9$) by integrating over different intervals in the angles θ_ℓ , θ_K , and ϕ for the $B \rightarrow K^* \mu^+ \mu^-$ decay as

follows:

$$\begin{aligned}
A_3(q^2) &= \frac{\left[\int_{-\pi/4}^{\pi/4} - \int_{\pi/4}^{3\pi/4} + \int_{-3\pi/4}^{3\pi/4} - \int_{3\pi/4}^{7\pi/4} \right] d\phi \int_{-1}^1 d \cos \theta_K \int_{-1}^1 d \cos \theta_\ell \cdot I_{\text{sum}}(q^2, \theta_\ell, \theta_K, \phi)}{\int_0^{2\pi} d\phi \int_{-1}^1 d \cos \theta_K \int_{-1}^1 d \cos \theta_\ell \cdot I_{\text{sum}}(q^2, \theta_\ell, \theta_K, \phi)}, \\
A_4(q^2) &= \frac{\left[\int_0^{\pi/2} - \int_{\pi/2}^\pi + \int_0^\pi - \int_\pi^{2\pi} \right] d\phi \left[\int_0^1 - \int_{-1}^0 \right] d \cos \theta_K \left[\int_0^1 - \int_{-1}^0 \right] d \cos \theta_\ell \cdot I_{\text{sum}}(q^2, \theta_\ell, \theta_K, \phi)}{\int_0^{2\pi} d\phi \int_{-1}^1 d \cos \theta_K \int_{-1}^1 d \cos \theta_\ell \cdot I_{\text{sum}}(q^2, \theta_\ell, \theta_K, \phi)}, \\
A_5(q^2) &= \frac{\left[\int_0^{\pi/2} - \int_{\pi/2}^\pi + \int_0^\pi - \int_\pi^{2\pi} \right] d\phi \left[\int_0^1 - \int_{-1}^0 \right] d \cos \theta_K \int_{-1}^1 d \cos \theta_\ell \cdot I_{\text{diff}}(q^2, \theta_\ell, \theta_K, \phi)}{\int_0^{2\pi} d\phi \int_{-1}^1 d \cos \theta_K \int_{-1}^1 d \cos \theta_\ell \cdot I_{\text{sum}}(q^2, \theta_\ell, \theta_K, \phi)}, \\
A_9(q^2) &= \frac{\left[\int_0^{\pi/2} - \int_{\pi/2}^\pi + \int_0^\pi - \int_\pi^{2\pi} \right] d\phi \int_{-1}^1 d \cos \theta_K \int_{-1}^1 d \cos \theta_\ell \cdot I_{\text{diff}}(q^2, \theta_\ell, \theta_K, \phi)}{\int_0^{2\pi} d\phi \int_{-1}^1 d \cos \theta_K \int_{-1}^1 d \cos \theta_\ell \cdot I_{\text{sum}}(q^2, \theta_\ell, \theta_K, \phi)}, \tag{8}
\end{aligned}$$

with

$$\begin{aligned}
I_{\text{sum}}(q^2, \theta_\ell, \theta_K, \phi) &= I^{(\ell)}(q^2, \theta_\ell, \theta_K, \phi) + \bar{I}^{(\ell)}(q^2, \theta_\ell, \theta_K, \phi), \\
I_{\text{diff}}(q^2, \theta_\ell, \theta_K, \phi) &= I^{(\ell)}(q^2, \theta_\ell, \theta_K, \phi) - \bar{I}^{(\ell)}(q^2, \theta_\ell, \theta_K, \phi), \tag{9}
\end{aligned}$$

where the angular asymmetries A_i are related to the CP-averaged observables S_i ,² namely,

$$\begin{aligned}
A_3 &= \frac{1}{\pi} S_3, & A_4 &= \frac{1}{\pi} S_4, \\
A_5 &= \frac{3}{8} S_5, & A_9 &= \frac{1}{\pi} S_9. \tag{11}
\end{aligned}$$

Clearly, analogous to S_i [67, 71, 72], the observables A_i are also sensitive to NP. As a matter of fact, the relative uncertainties of observables A_i and those of S_i are equal. On the experimental side, these observables can be measured either by fitting to angular distributions, or by performing angular integrations of I_i . However, this may result in different statistical uncertainties because of different angular coverages. It should be noted that the observables A_i are ratios of combinations of the well-known angular coefficients I_i . Therefore it is feasible to measure them in the current experiments.

In addition to the A_i observables, following Refs. [5, 73], we revisit the ratios of angular observables R_i ,

$$R_i(q^2) = \frac{I_i^{(\mu)}(q^2) + \bar{I}_i^{(\mu)}(q^2)}{I_i^{(e)}(q^2) + \bar{I}_i^{(e)}(q^2)}, \tag{12}$$

which are defined with the angular coefficients in Eq. (6). As pointed out in Ref. [73], the observables R_i are sensitive to new physics and their hadronic uncertainties are almost exactly cancelled. It should be emphasized that in this work the lepton mass m_ℓ is non-vanishing and the angular coefficient I_0^c is absent because we do not consider scalar operators.

² The CP-averaged observables are introduced in Ref. [67] as

$$S_i(q^2) = \frac{I_i(q^2) + \bar{I}_i(q^2)}{d(\Gamma + \bar{\Gamma})/dq^2}. \tag{10}$$

III. RESULTS AND DISCUSSIONS

In this section, we first update the global fits of Ref. [9] by considering the latest measurements $R_{K_S^0}$ and $R_{K^{*+}}$ [13] and perform global fits for two more NP scenarios, in comparison with Ref. [9]. Next, we study whether with the four asymmetry observables A_i and the ratios R_i introduced in Refs. [5, 73], one can distinguish different one-dimensional NP scenarios.

A. Updated global fits

In the Appendix of Ref. [9], we have updated the clean fits insensitive to hadronic uncertainties by considering the latest measurements of $R_{K_S^0}$ and $R_{K^{*+}}$. It is shown that the three one-dimensional scenarios δC_9^μ , δC_{10}^μ and $\delta C_L^\mu = \delta C_9^\mu = -\delta C_{10}^\mu$ and a two-dimensional scenario $(\delta C_9^\mu, \delta C_{10}^\mu)$ can well describe the current experimental data. Interestingly, a likelihood ratio test favours the δC_L^μ scenario over the SM at 5σ significance. On the other hand, although the angular observables of the $B \rightarrow K^* \mu^+ \mu^-$ decay suffer from large hadronic uncertainties, they can still provide constraints on new physics. Therefore, it is interesting to study how the conclusions of the clean fits change when including these angular observables. For this purpose, we update the global fits of Ref. [9]. We should note that the total number of fitted data for the updated global fits is 96. We obtain $\chi_{\text{SM},\text{min}}^2 = 131.98$ with 96 degrees of freedom, corresponding to a p -value of 0.009. Compared to the global fits of Ref. [9], the updated fits given in Table I and Fig. 2 show that the confidence level of the exclusion of the SM predictions increases by $0.3\sigma \sim 0.38\sigma$ for all the NP scenarios. In particular, the significance of deviation from SM in the δC_L^μ scenario is more than 5σ as well. In addition, we find that the updated global fit constrains better δC_9^μ in the two-dimensional $(\delta C_9^\mu, \delta C_{10}^\mu)$ scenario and excludes positive values at 1σ confidence level, as shown in Fig. 2.

In fact, in the case of NP involving tree-level exchanges of new particles such as the neutral gauge boson Z' , leptoquarks or scalar Higgs, further correlations can be induced between the Wilson coefficients $C_9^{\mu(\prime)}$ and $C_{10}^{\mu(\prime)}$. As demonstrated in some model independent analyses [22, 55, 58–60, 63, 66], two additional one-dimensional scenarios $\delta C_9^{\mu\prime} = C_{10}^{\mu\prime}$ and $\delta C_9^{\mu\prime} = -C_{10}^{\mu\prime}$ cannot be completely excluded by the current $b \rightarrow s\ell\ell$ data. The former scenario can be realized in the U_1 leptoquark model in the case of $\mathbf{g}_{\ell q}^{\mu b} (\mathbf{g}_{\ell q}^{\mu s})^* = \mathbf{g}_{ed}^{\mu b} (\mathbf{g}_{ed}^{\mu s})^*$ [43]. The latter one could be realized in Z' models with vector-like fermions and $L_\mu - L_\tau$ symmetry [74]. Therefore, we would like to investigate these two NP scenarios in our theoretical framework. This can be done following the same strategy as that of Ref. [9] and the corresponding results are shown in Table I. We note that the $\delta C_9^{\mu\prime} = C_{10}^{\mu\prime}$ and $\delta C_9^{\mu\prime} = -C_{10}^{\mu\prime}$ scenarios can well explain the new $b \rightarrow s\ell\ell$ data and the deviation from the SM has a significance of more than 3σ , smaller than the three one-dimensional δC_9^μ ,

δC_{10}^μ and δC_L^μ scenarios. Indeed, we also tested the other one-dimensional scenarios induced by NP models with the new data studied in the present work and found that they are excluded at 3σ confidence level, consistent with the conclusions of Refs. [22, 55, 58–60, 63, 66].

TABLE I. Best fit values, χ_{\min}^2 , p -value, Pull_{SM} and confidence intervals of the WCs in the five one dimensional scenarios.

Coeff.	Best fit	χ_{\min}^2	P -value	Pull_{SM}	1σ range	3σ range
$\delta C_9^\mu = C_{10}^{\mu\prime}$	-0.49	118.75 [95 dof]	0.05	3.64	[-0.62, -0.35]	[-0.90, -0.09]
$\delta C_9^\mu = -C_9^{\mu\prime}$	-1.03	117.99 [95 dof]	0.06	3.74	[-1.31, -0.76]	[-1.91, -0.20]
δC_9^μ	-0.90	108.05 [95 dof]	0.17	4.89	[-1.11, -0.70]	[-1.55, -0.33]
δC_{10}^μ	0.57	109.64 [95 dof]	0.14	4.73	[0.45, 0.70]	[0.20, 0.98]
δC_L^μ	-0.42	104.00 [95 dof]	0.25	5.29	[-0.50, -0.34]	[-0.68, -0.18]
$(\delta C_9^\mu, \delta C_{10}^\mu)$	(-0.58, 0.32)	103.51 [94 d.o.f.]	0.24	4.97	$\delta C_9^\mu \in [-0.81, -0.34]$	$\delta C_{10}^\mu \in [0.17, 0.48]$

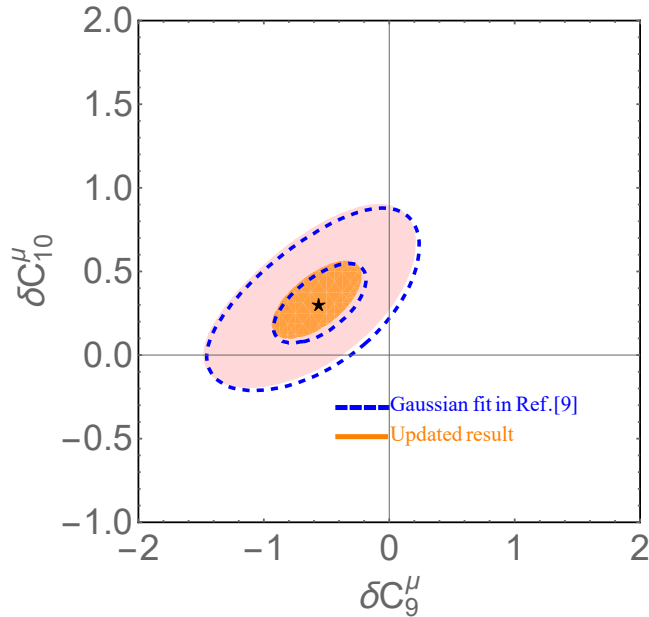


FIG. 2. Contour plots at the 1σ and 3σ confidence level for the $(\delta C_9^\mu, \delta C_{10}^\mu)$ scenario. The updated global fit with all observables for Gaussian (regions in light red and orange) is compared with the corresponding global fit of Ref. [9] (dashed lines in blue).

As discussed above, among the new NP scenarios studied, all of the five one-dimensional cases, i.e., δC_9^μ , δC_{10}^μ , δC_L^μ , $\delta C_9^\mu = C_{10}^{\mu\prime}$ and $\delta C_9^\mu = -C_9^{\mu\prime}$, can provide a good description of the latest data. Thus, a natural question is which observables can discriminate between them. For such a purpose, we study the four angular asymmetries A_i ($i = 3, 4, 5, 9$) and the ratios R_i introduced in Sec. II.

B. Sensitivity of angular asymmetries A_i to new physics

In Fig. 3, we plot $A_{3,5,4,9}$ as functions of q^2 , where q is the dilepton invariant mass, with the best fitted Wilson coefficients determined for the SM and the five one-dimensional NP scenarios. The shaded bands reflect the uncertainties originating from form factors and contributions of charm loops [5, 68, 73]. The asymmetries integrated over $[15,19]$ GeV² are given in Table II.

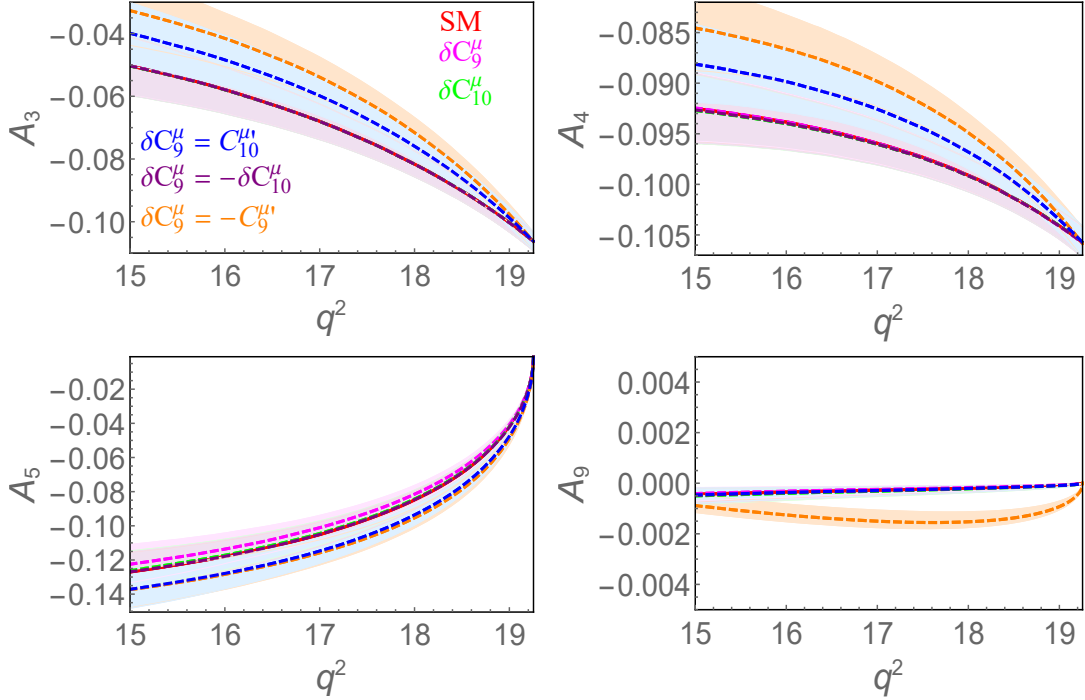


FIG. 3. Dilepton mass squared (q^2) spectra of observables A_i in the SM (solid lines in red) and different NP scenarios (dashed lines). Shaded regions denote the uncertainties of SM and five NP scenarios.

TABLE II. Predictions in the SM and five NP scenarios for binned observables.

Observables	SM	δC_9^μ	δC_{10}^μ	$\delta C_9^\mu = C_{10}^{\mu\prime}$	δC_L^μ	$\delta C_9^\mu = -C_9^{\mu\prime}$
A_3 [15,19] GeV ²	$-0.067^{+0.006}_{-0.006}$	$-0.067^{+0.006}_{-0.006}$	$-0.067^{+0.006}_{-0.006}$	$-0.060^{+0.007}_{-0.007}$	$-0.067^{+0.006}_{-0.006}$	$-0.054^{+0.007}_{-0.007}$
A_4 [15,19] GeV ²	$-0.096^{+0.002}_{-0.002}$	$-0.096^{+0.002}_{-0.002}$	$-0.096^{+0.002}_{-0.002}$	$-0.093^{+0.003}_{-0.002}$	$-0.096^{+0.002}_{-0.002}$	$-0.090^{+0.003}_{-0.003}$
A_5 [15,19] GeV ²	$-0.104^{+0.008}_{-0.008}$	$-0.101^{+0.008}_{-0.008}$	$-0.104^{+0.008}_{-0.008}$	$-0.113^{+0.008}_{-0.008}$	$-0.104^{+0.008}_{-0.008}$	$-0.115^{+0.008}_{-0.008}$
A_9 [15,19] GeV ²	$-0.0003^{+0.0001}_{-0.0002}$	$-0.0003^{+0.0001}_{-0.0002}$	$-0.0003^{+0.0002}_{-0.0002}$	$-0.0003^{+0.0002}_{-0.0002}$	$-0.0003^{+0.0002}_{-0.0002}$	$-0.0013^{+0.0004}_{-0.0002}$

By examining Fig. 3 and Table II, we can see that these observables can provide two possible strategies to distinguish between different NP structures. The first strategy is to analyse the q^2 spectra of certain observables. It is clear that the discriminating power of these observables $A_i(q^2)$ is very limited. For

instance, to distinguish the NP scenario $\delta C_9^\mu = -C_9^{\mu'}$, an experimental uncertainty of sub percent level or lower is needed. The second strategy is to study binned observables in proper ranges of q^2 . As shown in Table II, only binned A_3 and A_9 have the ability to discriminate the scenarios $\delta C_9^\mu = -C_9^{\mu'}$ and $\delta C_9^\mu = C_{10}^{\mu'}$ at 3σ confidence level if they can be measured with an uncertainty of 0.001. However, the other NP scenarios cannot be discriminated by these observables A_i .

In conclusion, the angular asymmetries A_i cannot uniquely distinguish between the five different NP solutions in the one-dimensional scenario.

C. Sensitivity of ratios R_i to new physics

In this subsection, we study whether the ratios R_i introduced in Refs. [5, 73] can be used to discriminate the five NP scenarios.

First we plot the q^2 spectra of $R_i(q^2)$ in the low bin of [0.045,6] GeV² in Fig. 4. One can see that the two observable $R_{1s}(q^2)$ and $R_{2s}(q^2)$ could discriminate all the five different NP scenarios, while the observable $R_{1c}(q^2)$ or $R_{2c}(q^2)$ can only discriminate the NP scenario $\delta C_9^\mu = -C_9^{\mu'}$. As explicitly shown in Appendix B, the other ratios suffer from uncertainties induced by power corrections and charm loop contributions and have no ability to distinguish the NP scenarios. We stress that it is possible to distinguish the five different NP scenarios if future experimental statistics is high enough such that an uncertainty of percent level or lower can be achieved.

TABLE III. Same as Table. II but for observables $R_{1c,1s,2c,2s,C,S}$.

Observables	SM	δC_9^μ	δC_{10}^μ	$\delta C_9^\mu = C_{10}^{\mu'}$	δC_L^μ	$\delta C_9^\mu = -C_9^{\mu'}$
R_{1s} [1,4] GeV ²	0.982 ^{+0.002} _{-0.002}	1.14 ^{+0.02} _{-0.03}	0.84 ^{+0.03} _{-0.02}	1.06 ^{+0.03} _{-0.03}	0.94 ^{+0.03} _{-0.03}	1.19 ^{+0.02} _{-0.03}
R_{2s} [1,4] GeV ²	0.966 ^{+0.001} _{-0.001}	1.12 ^{+0.01} _{-0.02}	0.83 ^{+0.02} _{-0.02}	1.04 ^{+0.02} _{-0.03}	0.92 ^{+0.02} _{-0.03}	1.17 ^{+0.02} _{-0.02}
R_{1c} [1,6] GeV ²	1.007 ^{+0.001} _{-0.001}	0.83 ^{+0.02} _{-0.01}	0.85 ^{+0.02} _{-0.02}	0.77 ^{+0.02} _{-0.01}	0.80 ^{+0.01} _{-0.01}	0.68 ^{+0.06} _{-0.03}
R_{2c} [1,6] GeV ²	0.977 ^{+0.001} _{-0.001}	0.81 ^{+0.02} _{-0.01}	0.83 ^{+0.02} _{-0.02}	0.75 ^{+0.02} _{-0.01}	0.78 ^{+0.01} _{-0.01}	0.66 ^{+0.05} _{-0.03}
R_S [1,4] GeV ²	0.985 ^{+0.003} _{-0.002}	1.14 ^{+0.02} _{-0.03}	0.84 ^{+0.03} _{-0.02}	1.07 ^{+0.03} _{-0.03}	0.95 ^{+0.03} _{-0.03}	1.19 ^{+0.02} _{-0.03}
R_C [1,6] GeV ²	0.9994 ^{+0.0007} _{-0.0008}	0.82 ^{+0.02} _{-0.01}	0.85 ^{+0.02} _{-0.02}	0.77 ^{+0.02} _{-0.01}	0.80 ^{+0.01} _{-0.01}	0.68 ^{+0.06} _{-0.03}

Next, we study binned observables in proper ranges of q^2 . As shown in Table III, once R_{1s} or R_{2s} is measured with the same accuracy as that of theoretical predictions, the five different NP scenarios can be either confirmed or excluded at 2σ confidence level. Therefore, the binned observables R_{1s} and R_{2s} are useful to distinguish between different NP scenarios, though less constraining than the q^2 spectra. We

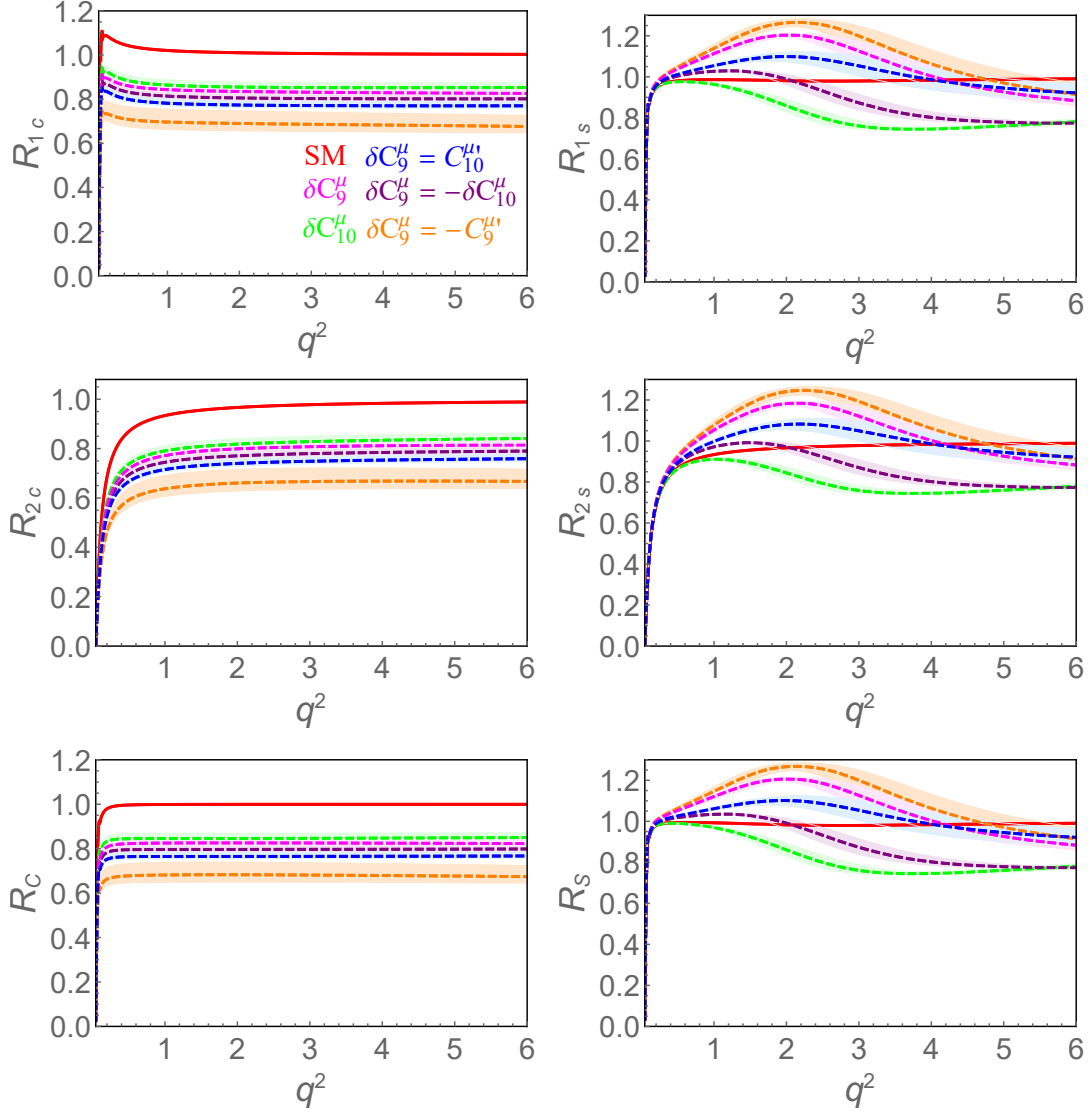


FIG. 4. Same as Fig. 3 but for observables $R_{1c,1s,2c,2s,C,S}$.

therefore conclude that the ratios R_{1s} and R_{2s} could uniquely distinguish between the five different NP solutions in the one-dimensional scenario if they can be measured with a precision of percent level.

On the experimental side, the angular coefficients I_{1s} and I_{2s} are not directly measured. Instead, the measured quantities are the branching ratio BR and the longitudinal polarization F_L as combinations of I_{1c} , I_{1s} , I_{2c} , and I_{2s} , which read

$$\frac{d\text{BR}}{dq^2} = \frac{\tau_B}{2} \frac{d(\Gamma + \bar{\Gamma})}{dq^2} = \frac{\tau_B}{4} \left[(3\Sigma_{1c}(q^2) - \Sigma_{2c}(q^2)) + 2(3\Sigma_{1s}(q^2) - \Sigma_{2s}(q^2)) \right], \quad (13)$$

$$F_L = \frac{1}{2} \frac{3\Sigma_{1c}(q^2) - \Sigma_{2c}(q^2)}{d(\Gamma + \bar{\Gamma})/dq^2}, \quad (14)$$

where

$$\Sigma_{1s,1c,2s,2c}(q^2) = I_{1s,1c,2s,2c}(q^2) + \bar{I}_{1s,1c,2s,2c}(q^2). \quad (15)$$

Clearly, the four angular coefficients I_{1c} , I_{1s} , I_{2c} , and I_{2s} cannot be uniquely determined by two observables BR and F_L . However, we note that two combinations of angular coefficients $3\Sigma_{1c} - \Sigma_{2c}$ and $3\Sigma_{1s} - \Sigma_{2s}$ can be extracted from BR and F_L . Therefore, we define two new ratios

$$R_C(q^2) = \frac{3\Sigma_{1c}^\mu(q^2) - \Sigma_{2c}^\mu(q^2)}{3\Sigma_{1c}^e(q^2) - \Sigma_{2c}^e(q^2)}, \quad (16)$$

$$R_S(q^2) = \frac{3\Sigma_{1s}^\mu(q^2) - \Sigma_{2s}^\mu(q^2)}{3\Sigma_{1s}^e(q^2) - \Sigma_{2s}^e(q^2)}. \quad (17)$$

It should be feasible to extract them experimentally. Therefore, we study the q^2 spectra and binned values of $R_{C,S}(q^2)$ in the SM and different NP scenarios. The relevant results are shown in Table III and Fig. 4. It is clear that the ratio R_S could uniquely distinguish between the five different NP solutions in the one-dimensional scenario if it can be measured with a precision of percent level.

IV. SUMMARY AND OUTLOOK

In conclusion, in the one-dimensional NP case only five scenarios, i.e., δC_9^μ , δC_{10}^μ , δC_L^μ , $\delta C_9^\mu = C_{10}^{\mu\prime}$ and $\delta C_9^\mu = -C_9^{\mu\prime}$, can well describe the latest LHCb, Belle, ATLAS, and CMS data. In order to discriminate the five different NP scenarios, we first ‘‘constructed’’ four angular asymmetries A_i and study the sensitivity of A_i to new physics. We find that these observables A_i cannot discriminate different NP scenarios. Further, we constructed a new ratio R_S by revisiting a set of ratios R_i and showed that the observable R_S can uniquely discriminate the five NP solutions in the one-dimensional case once they are measured in future experiments, by analysing the q^2 spectra of these observables and their binned results.

In the next few years, with the collection of more data at the LHCb, Belle II experiments and improvement of experimental precision, such global fits should be continually updated. In addition, new ideas should be explored to further reduce hadronic uncertainties. Furthermore, it will be interesting to study the interplay between semi-leptonic baryon decays, such as $\Lambda_b \rightarrow \Lambda$, $\Xi_b \rightarrow \Xi$, and semi-leptonic meson decays. Because of rich helicity structures, if measured up to the same precision, semi-leptonic baryon decays could constrain more tightly some relevant Wilson coefficients than their mesonic counterparts.

V. ACKNOWLEDGMENTS

We thank Jorge Martin Camalich for providing the code for the calculation of the $b \rightarrow s\ell\ell$ amplitudes. This work is partly supported by the National Natural Science Foundation of China under Grants

No.11735003, No.11975041, and No.11961141004, and the fundamental Research Funds for the Central Universities.

VI. APPENDIX

A. Discussion about NP in the electron and muon channels

In our current work and most works performed so far, NP is assumed to only originate from the muon mode. On the other hand, one can also assume that NP exists in the electron mode, or a combination of the electron and muon modes. In the electron mode, the signs of the fitted Wilson coefficients should be opposite to those of the muon mode if only the observables R_K and R_{K^*} are taken into account. The case of allowing for NP in the electron channel has been discussed quite extensively in Refs. [62, 75] (for some recent studies see, e.g., Refs. [55, 58, 76–78]). Here, we investigate a more general scenario that NP comes from a combination of electron and muon channels. As a result, more experimental data need to be taken into account, such as the branching fraction [79] as well as eight angular observables [80, 81] for the $B \rightarrow K^* e^+ e^-$ decay. Thus, the total number of data fitted becomes 103.

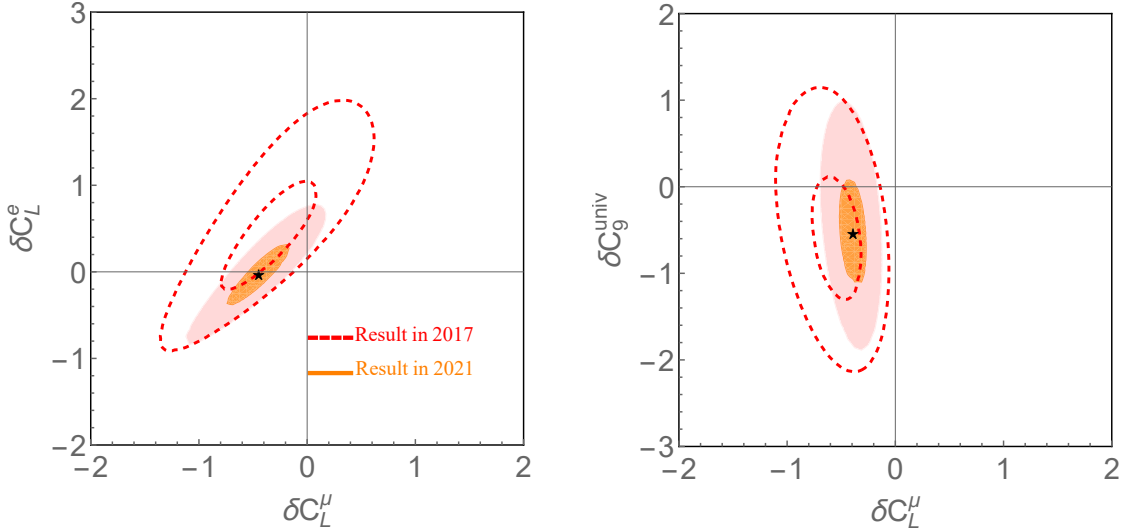


FIG. 5. Contours for the two-parameter fits $(\delta C_L^\mu, \delta C_L^e)$ and $(\delta C_L^\mu, \delta C_9^{\text{univ}})$ including the full data set (103 data). The regions in orange and light-red represent the 1σ and 3σ bounds. The lines in red correspond to those in Fig.7 of Ref. [5].

In Fig. 5, we show the two-parameter fits for the $(\delta C_L^\mu, \delta C_L^e)$ and $(\delta C_L^\mu, \delta C_9^{\text{univ}})$ cases including the full 103 data set. Here, one requires $\delta C_9^{\text{univ}} = \delta C_9^\mu = \delta C_9^e$. Compared to the results in 2017, all the NP scenarios are better constrained as shown by the smaller contours. In addition, the pure δC_L^{univ} scenario does

not change significantly and is still in agreement with the SM within the 1σ confidence level while other scenarios are not. More specifically, the significance of the SM exclusion in the pure δC_L^μ scenario becomes larger. Also, the new data favor a zero δC_9^e contribution. It should be mentioned that these variations from 2017 to 2021 are mainly caused by the most precise R_K from the LHCb experiment. The results indicate that new physics is most likely to exist in the muon mode.

B. q^2 spectra of R_{3-9}

In Fig. 5, we show the q^2 spectra of R_{3-9} . Clearly, these ratios cannot discriminate the five NP scenarios.

-
- [1] S. L. Glashow, J. Iliopoulos, and L. Maiani, *Phys. Rev. D* **2**, 1285 (1970).
 - [2] Y. Li and C.-D. Lü, *Sci. Bull.* **63**, 267 (2018), arXiv:1808.02990 [hep-ph].
 - [3] S. Bifani, S. Descotes-Genon, A. Romero Vidal, and M.-H. Schune, *J. Phys.* **G46**, 023001 (2019), arXiv:1809.06229 [hep-ex].
 - [4] R. Aaij et al. (LHCb), (2021), arXiv:2103.11769 [hep-ex].
 - [5] L.-S. Geng, B. Grinstein, S. Jäger, J. Martin Camalich, X.-L. Ren, and R.-X. Shi, *Phys. Rev.* **D96**, 093006 (2017), arXiv:1704.05446 [hep-ph].
 - [6] R. Aaij et al. (LHCb), *Phys. Rev. Lett.* **113**, 151601 (2014), arXiv:1406.6482 [hep-ex].
 - [7] R. Aaij et al. (LHCb), (2021), arXiv:2108.09283 [hep-ex].
 - [8] R. Aaij et al. (LHCb), (2021), arXiv:2108.09284 [hep-ex].
 - [9] L.-S. Geng, B. Grinstein, S. Jäger, S.-Y. Li, J. Martin Camalich, and R.-X. Shi, *Phys. Rev. D* **104**, 035029 (2021), arXiv:2103.12738 [hep-ph].
 - [10] M. Beneke, C. Bobeth, and R. Szafron, *JHEP* **10**, 232 (2019), arXiv:1908.07011 [hep-ph].
 - [11] A. M. Sirunyan et al. (CMS), *JHEP* **04**, 188 (2020), arXiv:1910.12127 [hep-ex].
 - [12] M. Aaboud et al. (ATLAS), *JHEP* **04**, 098 (2019), arXiv:1812.03017 [hep-ex].
 - [13] R. Aaij et al. (LHCb), (2021), arXiv:2110.09501 [hep-ex].
 - [14] A. Abdesselam et al. (Belle), *Phys. Rev. Lett.* **126**, 161801 (2021), arXiv:1904.02440 [hep-ex].
 - [15] S. Choudhury et al. (BELLE), *JHEP* **03**, 105 (2021), arXiv:1908.01848 [hep-ex].
 - [16] R. Aaij et al. (LHCb), *Phys. Rev. Lett.* **125**, 011802 (2020), arXiv:2003.04831 [hep-ex].
 - [17] R. Aaij et al. (LHCb), *Phys. Rev. Lett.* **126**, 161802 (2021), arXiv:2012.13241 [hep-ex].
 - [18] R. Aaij et al. (LHCb), *JHEP* **02**, 104 (2016), arXiv:1512.04442 [hep-ex].
 - [19] W. Altmannshofer and P. Stangl, *Eur. Phys. J. C* **81**, 952 (2021), arXiv:2103.13370 [hep-ph].
 - [20] C. Cornella, D. A. Faroughy, J. Fuentes-Martin, G. Isidori, and M. Neubert, *JHEP* **08**, 050 (2021), arXiv:2103.16558 [hep-ph].

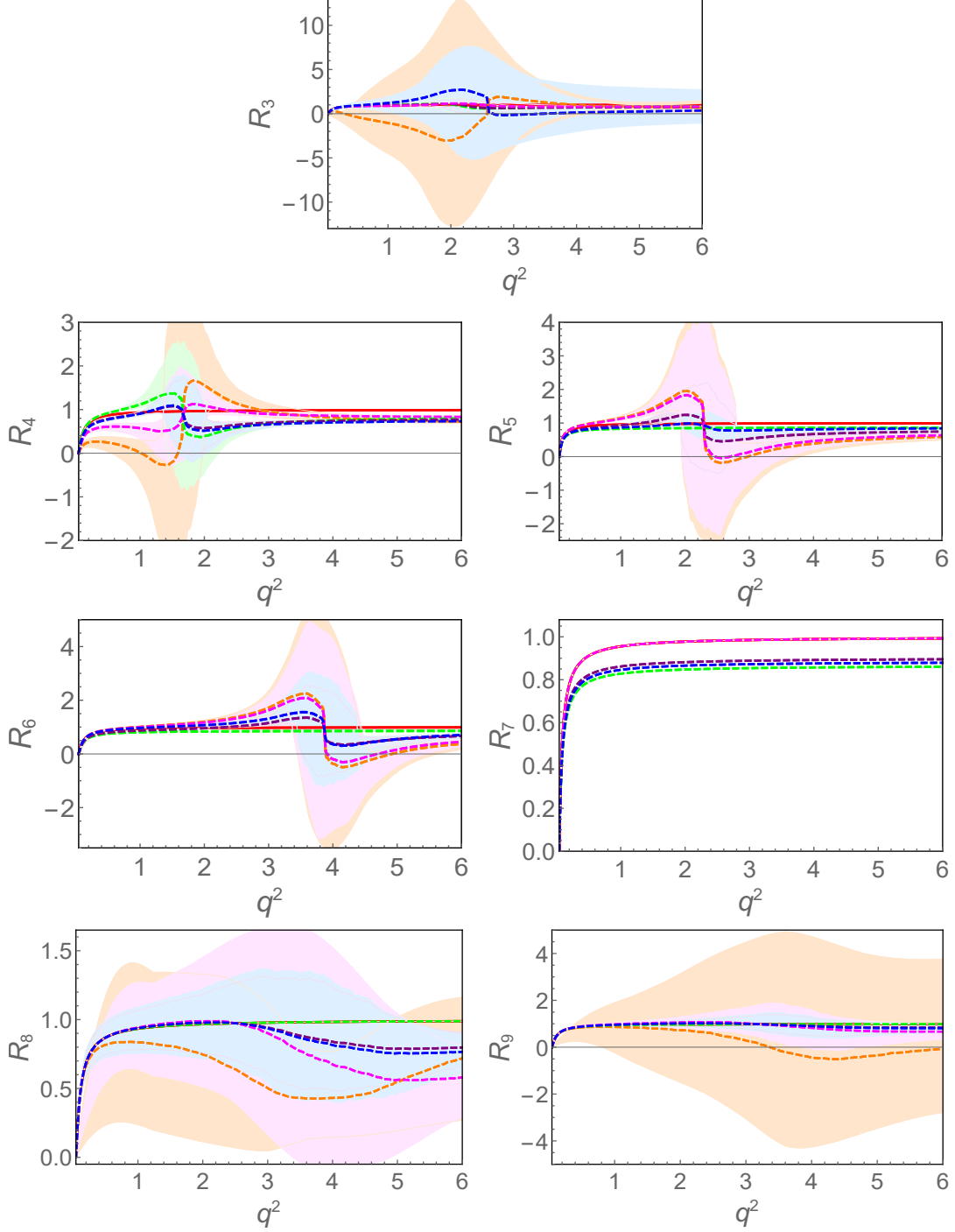


FIG. 6. Same as Fig. 4 but for observables R_{3-9} .

- [21] J. Kriewald, C. Hati, J. Orloff, and A. M. Teixeira, in 55th Rencontres de Moriond on Electroweak Interactions and Unified Theories (2021) arXiv:2104.00015 [hep-ph].
- [22] M. Algueró, B. Capdevila, S. Descotes-Genon, J. Matias, and M. Novoa-Brunet, in 55th Rencontres de Moriond on QCD and High Energy Interactions (2021) arXiv:2104.08921 [hep-ph].
- [23] T. Hurth, F. Mahmoudi, D. M. Santos, and S. Neshatpour, (2021), arXiv:2104.10058 [hep-ph].

- [24] A. Carvunis, F. Dettori, S. Gangal, D. Guadagnoli, and C. Normand, (2021), arXiv:2102.13390 [hep-ph].
- [25] A. Angelescu, D. Bečirević, D. A. Farouhy, F. Jaffredo, and O. Sumensari, Phys. Rev. D **104**, 055017 (2021), arXiv:2103.12504 [hep-ph].
- [26] G. Isidori, D. Lancierini, P. Owen, and N. Serra, Phys. Lett. B **822**, 136644 (2021), arXiv:2104.05631 [hep-ph].
- [27] J. Alda, J. Guasch, and S. Penaranda, in European Physical Society Conference on High Energy Physics 2021 (2021) arXiv:2110.12240 [hep-ph].
- [28] G. Isidori, D. Lancierini, A. Mathad, P. Owen, N. Serra, and R. S. Coutinho, (2021), arXiv:2110.09882 [hep-ph].
- [29] J.-P. Lee, (2021), arXiv:2110.05583 [hep-ph].
- [30] R. Bause, H. Gisbert, M. Golz, and G. Hiller, (2021), arXiv:2109.01675 [hep-ph].
- [31] J.-Y. Cen, Y. Cheng, X.-G. He, and J. Sun, (2021), arXiv:2104.05006 [hep-ph].
- [32] J. Kawamura and S. Raby, Phys. Rev. D **104**, 035007 (2021), arXiv:2104.04461 [hep-ph].
- [33] B. C. Allanach, J. M. Butterworth, and T. Corbett, (2021), arXiv:2110.13518 [hep-ph].
- [34] A. K. Alok, N. R. S. Chundawat, and D. Kumar, (2021), arXiv:2110.12451 [hep-ph].
- [35] P. Ko, T. Nomura, and H. Okada, (2021), arXiv:2110.10513 [hep-ph].
- [36] M. F. Navarro and S. F. King, (2021), arXiv:2109.08729 [hep-ph].
- [37] R. Bause, G. Hiller, T. Höhne, D. F. Litim, and T. Steudtner, (2021), arXiv:2109.06201 [hep-ph].
- [38] A. K. Alok, A. Dighe, S. Gangal, and J. Kumar, (2021), arXiv:2108.05614 [hep-ph].
- [39] X. Wang, (2021), arXiv:2108.01279 [hep-ph].
- [40] J. Davighi, JHEP **08**, 101 (2021), arXiv:2105.06918 [hep-ph].
- [41] A. Greljo, P. Stangl, and A. E. Thomsen, Phys. Lett. B **820**, 136554 (2021), arXiv:2103.13991 [hep-ph].
- [42] T. Nomura and H. Okada, Phys. Rev. D **104**, 035042 (2021), arXiv:2104.03248 [hep-ph].
- [43] M. Du, J. Liang, Z. Liu, and V. Q. Tran, (2021), arXiv:2104.05685 [hep-ph].
- [44] P. F. Perez, C. Murgui, and A. D. Plascencia, Phys. Rev. D **104**, 035041 (2021), arXiv:2104.11229 [hep-ph].
- [45] A. Greljo, Y. Soreq, P. Stangl, A. E. Thomsen, and J. Zupan, (2021), arXiv:2107.07518 [hep-ph].
- [46] S. F. King, (2021), arXiv:2106.03876 [hep-ph].
- [47] S. Singirala, S. Sahoo, and R. Mohanta, (2021), arXiv:2106.03735 [hep-ph].
- [48] W.-F. Chang, JHEP **09**, 043 (2021), arXiv:2105.06917 [hep-ph].
- [49] K. Ban, Y. Jho, Y. Kwon, S. C. Park, S. Park, and P.-Y. Tseng, (2021), arXiv:2104.06656 [hep-ph].
- [50] D. Marzocca and S. Trifinopoulos, Phys. Rev. Lett. **127**, 061803 (2021), arXiv:2104.05730 [hep-ph].
- [51] H. M. Lee, Phys. Rev. D **104**, 015007 (2021), arXiv:2104.02982 [hep-ph].
- [52] J. Chen, Q. Wen, F. Xu, and M. Zhang, (2021), arXiv:2104.03699 [hep-ph].
- [53] W.-F. Duan, S.-P. Li, X.-Q. Li, and Y.-D. Yang, (2021), arXiv:2111.05178 [hep-ph].
- [54] K. S. Babu, P. S. B. Dev, S. Jana, and A. Thapa, JHEP **03**, 179 (2021), arXiv:2009.01771 [hep-ph].
- [55] A. K. Alok, A. Dighe, S. Gangal, and D. Kumar, JHEP **06**, 089 (2019), arXiv:1903.09617 [hep-ph].
- [56] F. Munir Bhutta, Z.-R. Huang, C.-D. Lü, M. A. Paracha, and W. Wang, (2020), arXiv:2009.03588 [hep-ph].

- [57] A. K. Alok, S. Kumbhakar, J. Saini, and S. U. Sankar, Nucl. Phys. B **967**, 115419 (2021), arXiv:2011.14668 [hep-ph].
- [58] J. Kumar and D. London, Phys. Rev. **D99**, 073008 (2019), arXiv:1901.04516 [hep-ph].
- [59] A. K. Alok, B. Bhattacharya, D. Kumar, J. Kumar, D. London, and S. U. Sankar, Phys. Rev. D **96**, 015034 (2017), arXiv:1703.09247 [hep-ph].
- [60] B. Capdevila, A. Crivellin, S. Descotes-Genon, J. Matias, and J. Virto, JHEP **01**, 093 (2018), arXiv:1704.05340 [hep-ph].
- [61] M. Algueró, P. A. Cartelle, A. M. Marshall, P. Masjuan, J. Matias, M. A. McCann, M. Patel, K. A. Petridis, and M. Smith, (2021), arXiv:2107.05301 [hep-ph].
- [62] T. Hurth, F. Mahmoudi, D. Martinez Santos, and S. Neshatpour, Phys. Rev. **D96**, 095034 (2017), arXiv:1705.06274 [hep-ph].
- [63] B. Capdevila, S. Descotes-Genon, J. Matias, and J. Virto, JHEP **10**, 075 (2016), arXiv:1605.03156 [hep-ph].
- [64] W. Altmannshofer, P. Stangl, and D. M. Straub, Phys. Rev. D **96**, 055008 (2017), arXiv:1704.05435 [hep-ph].
- [65] S. Descotes-Genon, J. Matias, and J. Virto, Phys. Rev. D **88**, 074002 (2013), arXiv:1307.5683 [hep-ph].
- [66] S. Descotes-Genon, L. Hofer, J. Matias, and J. Virto, JHEP **06**, 092 (2016), arXiv:1510.04239 [hep-ph].
- [67] W. Altmannshofer, P. Ball, A. Bharucha, A. J. Buras, D. M. Straub, and M. Wick, JHEP **01**, 019 (2009), arXiv:0811.1214 [hep-ph].
- [68] S. Jäger and J. Martin Camalich, JHEP **05**, 043 (2013), arXiv:1212.2263 [hep-ph].
- [69] R. Mandal, R. Sinha, and D. Das, Phys. Rev. **D90**, 096006 (2014), arXiv:1409.3088 [hep-ph].
- [70] A. K. Alok, S. Kumbhakar, and S. Uma Sankar, (2020), arXiv:2001.04395 [hep-ph].
- [71] T. Hurth, F. Mahmoudi, and S. Neshatpour, Nucl. Phys. **B909**, 737 (2016), arXiv:1603.00865 [hep-ph].
- [72] S. Bhattacharya, A. Biswas, S. Nandi, and S. K. Patra, Phys. Rev. **D101**, 055025 (2020), arXiv:1908.04835 [hep-ph].
- [73] S. Jäger and J. Martin Camalich, Phys. Rev. **D93**, 014028 (2016), arXiv:1412.3183 [hep-ph].
- [74] W. Altmannshofer, S. Gori, M. Pospelov, and I. Yavin, Phys. Rev. D **89**, 095033 (2014), arXiv:1403.1269 [hep-ph].
- [75] M. Ciuchini, A. M. Coutinho, M. Fedele, E. Franco, A. Paul, L. Silvestrini, and M. Valli, Eur. Phys. J. **C77**, 688 (2017), arXiv:1704.05447 [hep-ph].
- [76] M. Ciuchini, A. M. Coutinho, M. Fedele, E. Franco, A. Paul, L. Silvestrini, and M. Valli, Eur. Phys. J. **C79**, 719 (2019), arXiv:1903.09632 [hep-ph].
- [77] M. Algueró, B. Capdevila, S. Descotes-Genon, P. Masjuan, and J. Matias, Phys. Rev. **D99**, 075017 (2019), arXiv:1809.08447 [hep-ph].
- [78] M. Algueró, B. Capdevila, S. Descotes-Genon, P. Masjuan, and J. Matias, JHEP **07**, 096 (2019), arXiv:1902.04900 [hep-ph].
- [79] R. Aaij et al. (LHCb), JHEP **05**, 159 (2013), arXiv:1304.3035 [hep-ex].
- [80] R. Aaij et al. (LHCb), JHEP **04**, 064 (2015), arXiv:1501.03038 [hep-ex].
- [81] R. Aaij et al. (LHCb), JHEP **12**, 081 (2020), arXiv:2010.06011 [hep-ex].